COMPARING HYPERSPECTRAL AND THERMAL UAV-BORNE IMAGERY FOR RELATIVE WATER CONTENT ESTIMATION IN FIELD-GROWN SESAME

Maitreya Mohan Sahoo* and Rom Tarshish

The Robert H. Smith Faculty of Agriculture, Food and Environment, The Hebrew University of Jerusalem, Rehovot 7610001, Israel

Victor Alchanatis
Institute of Agricultural Engineering, Agricultural Research Organization (ARO) - Volcani Institute, Ministry of Agriculture and Rural Development, P.O. Box 6, Bet Dagan 50250, Israel

Ittai Herrmann
The Robert H. Smith Faculty of Agriculture, Food and Environment, The Hebrew University of Jerusalem, Rehovot 7610001, Israel

*Correspondence: maitreya.sahoo@mail.huji.ac.il

A paper from the Proceedings of the
16th International Conference on Precision Agriculture
21-24 July 2024
Manhattan, Kansas, United States

Abstract.

Sesame (Sesamum indicum) is an irrigated oilseed crop, and studies on its water content estimation are sparred. Unmanned aerial vehicle (UAV)-borne imagery using spectral reflectance as well as thermal emittance for crops are an ample source of high throughput phenotypic information about their physiological and chemical traits. Though several studies have dealt with thermal emittance to assess the crop water content, evaluating its relation to the plant's solar reflectance is limitedly explored. In this work, we remotely estimated the leaf relative water content (RWC) of field-grown sesame plants using hyperspectral and thermal UAV-borne imagery and discussed its trends for a growing season. Measurements were obtained for RWC by leaf destructive analysis for 20 field-grown sesame plots on sandy soil at five different dates throughout the season. It was followed by implementing paradigms of RWC estimation techniques using UAV-borne hyperspectral imagery in the range of 400 to 1000 nm and thermal infrared emittance data acquired from the crop canopies. The estimated RWC values were compared with the measured values to assess the quality of the estimation models. In a parallel set of analyses, we developed a relation between the measured RWC and thermal infrared-derived crop water stress index (CWSI) for sesame canopy. With RWC values ranging from 75 % to 90 %, it was observed that the genetic algorithm-based partial least square

regression (GA-PLSR) performed accurately using crop canopy hyperspectral reflectance for estimating RWC values along the full-time scale of acquisition with a cross-validated coefficient of determination (R^2) of 0.6 and root mean squared error (RMSE) of 1.77 %. On the contrary, the thermal dataset-derived CWSI provided the best fit of R^2 = 0.3 and RMSE = 1.73 % only at the last measuring date. However, its overall time scale trend did not provide better predictions. The regression models further showed a reduction in the leaf RWC as time progressed. This was evidenced by an increasing negative slope from -0.7 to -10 between RWC and CWSI, which indicated a developing water stress. With prior knowledge about the relation of CWSI with water status parameters (RWC and leaf water potential), possibilities of its dependence on photosynthesis were further explored, revealing that the CWSI is also affected by photosynthesis even with a low RWC. The advantage of the high dimensional hyperspectral data was exploited because it learned a weighted combination of spectral features compared to thermal data, thereby improving RWC estimation. The insights obtained from these experiments further helped us to map the experimental sesame plots' images for their water content during the growing season. Further scope would combine the hyperspectral and thermal datasets to improve RWC estimation through multimodal analysis.

Keywords.
Airborne imagery, multimodal analysis, crop temperature, GA-PLSR, crop water stress index.

INTRODUCTION

Leaf relative water content

Leaf relative water content (RWC) is defined as the percentage composition of water present in a leaf. It is one of the essential measures of a crop's water status, providing information about physiological processes in the leaf stomata that is vital for crop growth and development. It determines the plant health, photosynthetic efficiency and also acts an indicator for water stress assessment (Ullah et al. 2012). In the agriculture domain, accurate estimation of leaf RWC helps in scheduling irrigation and also for yield estimation (Peñuelas et al. 1993, Peñuelas et al. 1997). Instantaneous water stress in a crop, if not adequately managed, can create long-term water stress, resulting in a significant reduction in its yield (Hsiao and Acevedo 1974). Further the irrigation patterns can be monitored easily by the crop water status rather than measuring soil water content (Alchanatis et al. 2010; Jackson 1982).

Leaf water content can be determined through invasive and non-invasive techniques. Invasive techniques (determining directly from a leaf sample) is time consuming and is laborious for commercial farms. RWC estimation based on crop temperature measurements using thermal infrared (TIR) thermometers though considered as an accurate, reliable and non-invasive technique, this has limitations to acquire uniform measurements for large commercial fields (Alchanatis et al. 2010). Also, daytime changes in the solar illumination might affect such measurements. This necessitates for a faster and robust RWC estimation approach that can be implemented for larger fields. Remote sensing-based techniques offers its potential to utilize remotely sensed information from field crops for estimation of water content and mapping of a crop's water status.

Remote estimation of leaf RWC

Various remote sensing techniques pertaining to visible (VIS, 400 – 700 nm), near infrared (NIR, 700 – 1200 nm), shortwave infrared (SWIR, 1200 – 2500 nm), mid infrared (3 – 5 μm), thermal and far infrared (7.5 – 15 μm) and microwave (2.5 – 8 cm), have been used for remote estimation of leaf RWC (Srikanth et al. 2020; Ceccato et al. 2001; Clevers et al. 2010; Fabre et al. 2010; Gao et al. 2015; Huang et al. 2015; Hunt et al. 2011; Merlin et al. 2010; Neinavaz et al. 2017; Raj et al. 2021; Yilmaz et al. 2008). Unlike remote sensing at long wavelength regions constrained by coarse spatial resolution that offer a limited availability of terrestrial spectral energy, hyperspectral remote sensing enjoys the advantage of capturing information within hundreds of narrow contiguous spectral bands providing valuable insights on interaction of incident solar energy with water molecules present in the leaves (~970, ~1200, ~1400, ~1940 nm) as described in the work of Curran 1989.

Several studies have been conducted to estimate leaf water content and monitor water status from remotely sensed hyperspectral imagery, but these have been studied on determinate crops such as maize and wheat having a defined growth cycle. A study to remotely estimate leaf RWC on an indeterminate crop has never been published. Our study focuses on spectral estimation of leaf RWC for an indeterminate crop, sesame (*Sesamum indicum*) using hyperspectral and thermal remote sensing for a comparative analyse, that would address the timeline trend of water status for crops with indeterminate growth.

Aim and objectives

This study aimed to comparatively analyze the leaf RWC estimated from UAV-hyperspectral reflectance and thermal imagery for mapping water status in sesame field. To achieve this aim, specific objectives were set to be strived at:

1. To remotely estimate sesame leaf RWC from hyperspectral and thermal datasets.
2. To comparatively analyze between the measured leaf RWC and its estimates derived from hyperspectral and thermal imagery.

METHODOLOGY

Study area

Field experiment was conducted for the sesame crop in the Experimental Farm of The Robert H. Smith Faculty of Agriculture, Food and Environment, Rehovot, Israel (31°54'N; 34°48'E) during the summer of 2020 (Fig. 1(a)).

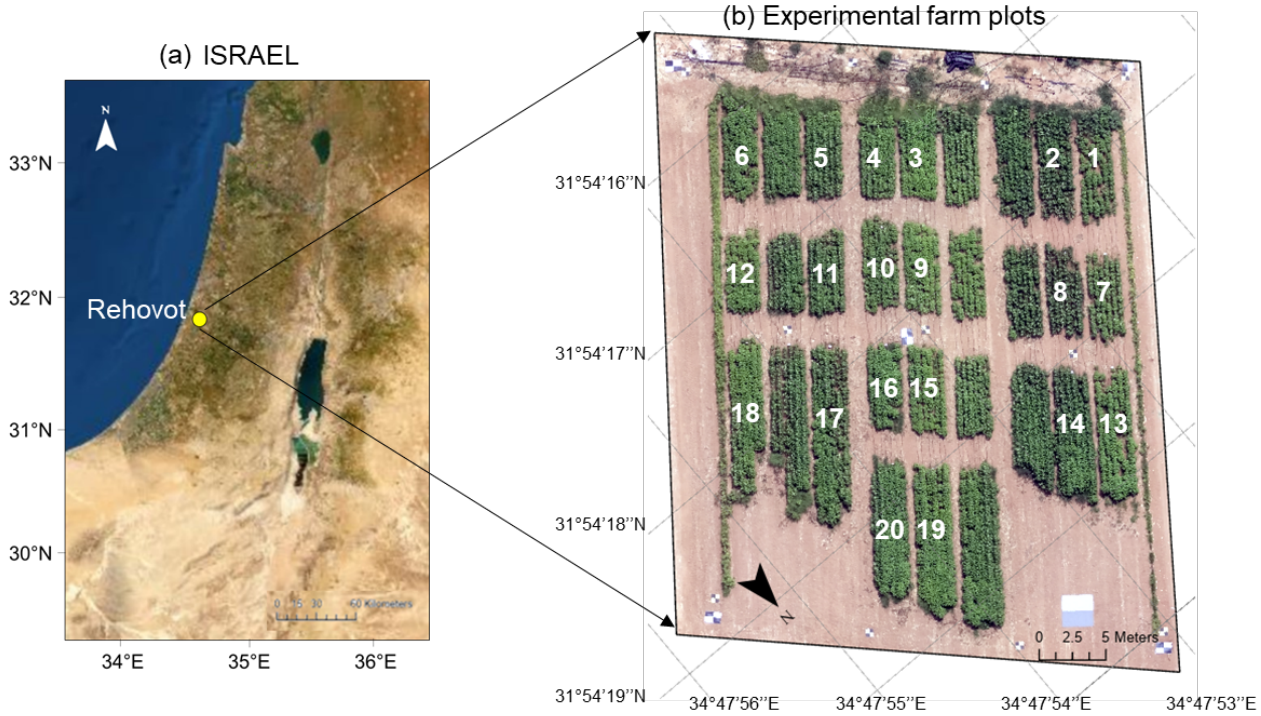

Fig 1. Study area of our experiment: (a) Field experiment was conducted at the experimental farm of The Robert H. Smith Faculty of Agriculture, Food and Environment in Rehovot; (b) Experimental farm plots displaying the selected sesame plots (highlighted by numbers in white color) used for our experiment.

Experiment and data acquisition

Sesame seeds of a single cultivar were sown on 24 May, 2020 in 30 plots of the experimental farm (Fig. 1(b)). Each plot had an average area of 14 m^2 (7 m long and 2 m wide), with a cropping density of 17 plants/m^2.

Post-emergence of plants on 31 May, 2020, remotely sensed data and leaf RWC were acquired at five dates during the growing season 39, 51, 57, 74 and 81 days after emergence (DAE).

- Sesame canopy hyperspectral reflectance images were acquired in the visible and near infrared (VNIR) region (385 – 1020 nm) using a Pika L airborne hyperspectral scanner (Resonon Inc. Bozeman, MT, USA) that was mounted on a Matrice600 UAV (DJI, Shenzhen, Guangdong, China). The hyperspectral scanner was deployed at an altitude of 100 m above canopy, with a field-of-view (FOV) of 24.8° (linear FOV 42 m) configured for obtaining 900 pixels per scanning line in 300 hyperspectral bands.
- TIR emittance images were acquired using an A655SC infrared camera (FLIR Systems, Melvile, NY, USA) mounted on a Matrice600 UAV. The camera had a spatial resolution of 640 × 480 pixels, sensitive in the spectral range of 7.5 µm – 13 µm.
- Leaf RWC was measured for youngest fully developed leaf picked from the centre of each sesame plot. The leaf samples were cut to ten circular discs of 0.8 cm diameter and weighed. It was followed by oven-drying them for 72 hours with the temperature set to 60 °C. Subsequently, the oven-dried leaf discs were weighed and the difference of the dry weight from the fresh weight was determined for each disc. The differences for ten leaf discs were averaged which determined the RWC of the leaf corresponding to the sesame

plot.

Data pre-processing

The UAV-borne hyperspectral images were pre-processed for:

1. Radiometric correction- Implemented using the Spectronon software with the calibration parameters provided by the manufacturer, Resonon, Inc.
2. Atmospheric correction- Implemented by flat field ratioing using a standard Resonon grey tarp.
3. Geometric correction- Mosaicking scanned lines to produce the hyperspectral image, followed by georectification.
4. Spatial subsetting- Subsetting obtained hyperspectral image to the areal coverage of the sesame field (shown in Fig. 1(b)).
5. Noise removal- The hyperspectral bands corresponding to 385 – 400 nm (bands 1 to 10) and 1010 – 1020 nm (bands 296 to 300) wavelength ranges were removed due to the high spectral noise present in them.
6. Spectral smoothening- The pre-processed hyperspectral images were spectrally smoothened for the 745 – 1010 nm (bands 174 to 295) wavelength range using the Savitzky-Golay method with a window size of 25 bands and polynomial value of 2 (Savitzky and Golay 1964).
7. Vegetation filtering- A normalized differential vegetation index (NDVI) threshold of 0.7 was set that distinguished vegetation (NDVI ≥ 7) from soil pixels (NDVI < 7). The NDVI is formulated as:

$$NDVI = \frac{\rho_{779.46} - \rho_{670.32}}{\rho_{779.46} + \rho_{670.32}} \geq 0.7$$

where $r_{779.46}$ and $r_{670.32}$ are the reflectance values at 779.46 nm and 670.32 nm corresponding to near infrared (NIR) and red bands, respectively.

The TIR images were pre-processed for spatial subsetting and extracting the vegetation pixels geographically co-registered with those of the hyperspectral reflectance images. It was followed by converting the digital number (DN) of the TIR pixels into crop water stress index (CWSI) values by normalization at a 0 – 1 scale (Alchanatis et al. 2010). The CWSI is formulated as:

$$CWSI = \frac{DN_{veg\_pxl} - min\,(DN_{veg\_pxls})}{min\left(DN_{veg\_pxls}\right) - max\left(DN_{veg\_pxls}\right)}$$

where DN_{veg_pxl} is the DN value of the vegetation-filtered TIR pixel, and $min\left(DN_{veg\_pxls}\right)$, $max\left(DN_{veg\_pxls}\right)$ are the minimum and maximum DN values among the vegetation-filtered pixels of the TIR image. CWSI images were derived from the TIR images for each data acquisition date using their corresponding DN value statistics.

The measured sesame leaf RWC was analysed for the presence of outliers (if any) using boxplots that identified outlier values as larger than 1.5 times from the interquartile range of the distribution (Langford 2006).

Data analysis

The processed sesame dataset for the experimental farm was analyzed for 20 selected plots (highlighted by white-colored plot numbers in Fig. 1(b)) to estimate their leaf RWC using paradigms of RWC estimation techniques.

UAV-borne images were used to determine correlation with the leaf RWC by using linear

regression modeled for each date of data acquisition. The hyperspectral and TIR-derived CWSI pixels corresponding to each sesame plot were averaged for a single hyperspectral reflectance and a mean CWSI value representing it. These averaged values linearly regressed for RWC provided us the Pearson's correlation coefficients (r) for each hyperspectral band and a linear fit with CWSI establishing the coefficient of determination (R^2).

The measured leaf RWC was analysed to identify hyperspectral two-wavelength combinations using normalized differential spectral indices (NDSIs) (Thenkabail et al. 2000; Sahoo et al. 2022) that highly correlates with it. The NDSI is formulated as:

$$NDSI_{(i,j)} = \frac{\rho_i - \rho_j}{\rho_i + \rho_j}$$

where i, j are the wavelengths, and ρ_i, ρ_j are their corresponding reflectance values.

The averaged hyperspectral reflectance was numerically modeled for the prediction of leaf RWC across all data acquisition dates using two machine learning (ML) techniques- (1) Random forest (RF) regression; and (2) Genetic algorithm-inspired partial least squares regression (GA-PLSR). RF is considered an accurate and robust ensemble technique for regression problems based on the aggregate result of decision trees to minimize the variance between measured values and their estimations. The RF model developed in our experiment was based on averaging the results for 100 epochs with each one of them trained on 70 % and cross-validated on 30 % randomly selected samples out of the total RWC measurements. Each epoch was trained using bootstrap and aggregation (aka Bagging) with a maximum 4 leaf node splits. The estimated leaf RWC from training and cross-validation were averaged for evaluating the model performance using R^2 and root mean squared error (RMSE) between the measured and estimated values.

Genetic algorithms have enhanced the performances of regression by selecting a subset of predictor features (individual hyperspectral bands in our case) and eliminating the noisy and highly correlated ones (Leardi et al. 1992). Discussed in the work of Leardi and Lupiáñez González 1998, the model is formulated as:

$$\hat{Y} = \beta_0 + \beta_1\rho_1 + \beta_2\rho_2 + \beta_3\rho_3 + \cdots + \beta_n\rho_n$$

with minimizing the error $\hat{Y} - Y$, where $\hat{Y}$ is the estimated RWC, Y is the measured RWC, ρ_1, ρ_2,…, ρ_n are the reflectance values of subset spectral bands. These bands are associated with weight coefficients β_1, β_2,…, β_n and β_0 is an estimated bias parameter for the model. GA-PLSR was performed for 100 epochs with the same training-testing set as used for RF regression to reduce the effect of sample distribution (Herrmann et al. 2018). The leaf RWC estimated from all epochs were averaged to evaluate the GA-PLSR performance using R^2 and RMSE metrics.

RESULTS

Linear regression

Linear regression model implemented for each hyperspectral band with the leaf RWC provided the spectral correlation with it (Fig. 2). The correlation coefficient corresponding to each wavelength revealed the RWC estimation trends for each date of data acquisition. It was observed that hyperspectral reflectance data acquired on 39 DAE displayed a weak correlation with RWC. 51 and 57 DAEs were featured with an improvement in correlation trend. The strongest correlation was observed on 57 DAE with a negative coefficient (r = -0.64) at 651.27 nm. Regression model of this wavelength provided a linear fit with R^2 = 0.37 and RMSE = 1.40 %. Post-57 DAE was observed a reduced correlation for subsequent measurement dates (74 and 81 DAEs).

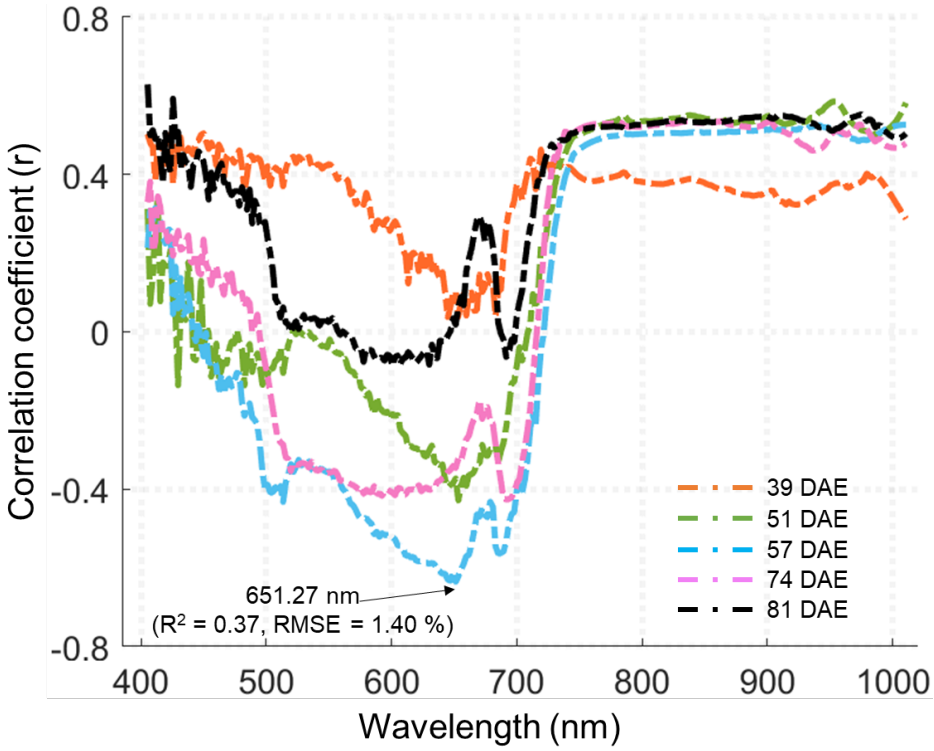

Fig 2. Pearson's correlation coefficient (r) determined for each hyperspectral wavelength linearly regressed with measured leaf RWC. The color for each correlation coefficient curve corresponds to each date of data acquisition. The wavelength with the strongest correlation has been indicated with its R^2 and RMSE values. DAE- Days after emergence; RWC- Relative water content; R^2- Coefficient of determination; RMSE- Root mean squared error.

Linear regression performed on CWSI revealed the trendlines estimating RWC for each data acquisition date (Fig. 3). The models displayed a progressive reduction of RWC with each TIR data acquisition date. Though a crop's water content is inversely related to its water stress, the rate of RWC reduction varies within its growing season (Raya-Sereno et al. 2024). This was evidenced by an increasing negative slope ranging from -0.7 to -10 between leaf RWC and CWSI, indicating a developing water stress. TIR-derived CWSI provided the best fit of R^2 = 0.30 and RMSE = 1.73 % on 74 DAE, a few days prior to sesame harvesting. Linear trends modeled on other acquisition dates did not provide better predictions.

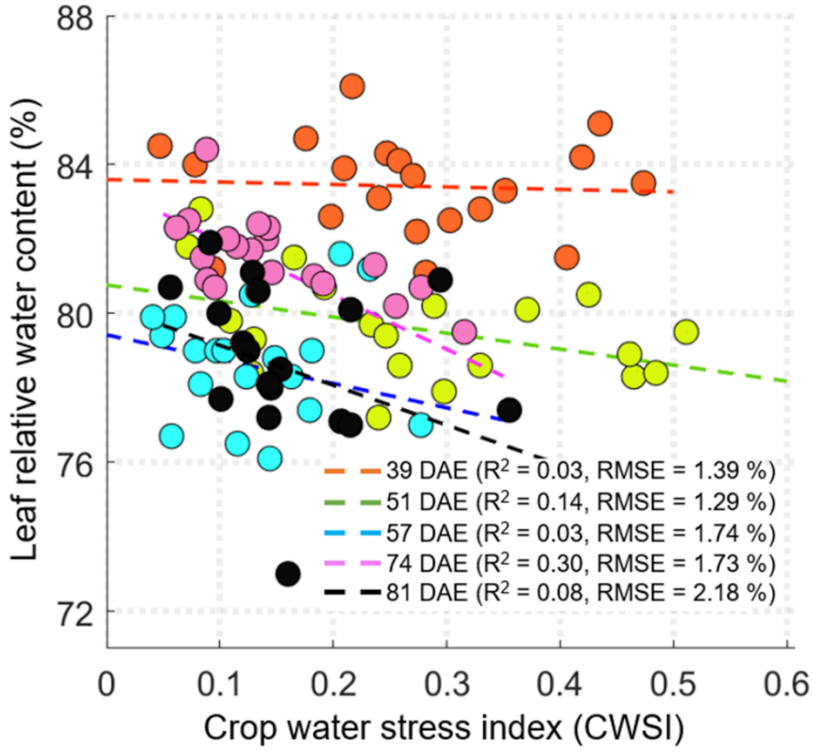

Fig 3. Trendlines of linear regression for estimating leaf RWC using TIR image-derived CWSI. The color for each linear trendline corresponds to its date of data acquisition. The R^2 and RMSE values are provided for each linear regression model. TIR- Thermal infrared; CWSI- Crop water stress index.

NDSI regression

The NDSI regression identified the two-wavelength combinations in hyperspectral datasets that were correlated with the RWC for each data acquisition date (Fig. 4). The initial days post-sesame emergence featured the red and blue region combinations that had maximum correlation with leaf water content. 39 DAE had the best linear fit (R^2 = 0.20, RMSE = 1.17 %) for 613.37-, 470.43 nm wavelength NDSI, while 51 DAE exhibited the same for 653.38, 431.73 nm combination (R^2 = 0.55, RMSE = 0.93 %). The highly correlated NDSI feature shifted towards the NIR and red wavelength combination (952.58, 727.84 nm) for 57 DAE with the strongest linear fit (R^2 = 0.60, RMSE = 1.11 %). Thereafter, the correlated NDSI features shifted towards the red-green region for 74 DAE (715.01, 540.39 nm with R^2 = 0.47, RMSE = 1.45 %) and 81 DAE (710.74, 556.99 nm with R^2 = 0.34, RMSE = 1.84 %). The NDSI regression trends revealed a determined fit only for one of the acquisition dates (57 DAE), which was also identified using linear regression for each hyperspectral band (Fig. 2). This showed a larger dependence on data acquisition date for spectral estimation of leaf RWC. This drawback was overcome with the use of ML techniques (RF and GA-PLSR) that learned the temporal variation among spectral features diagnostic to water content estimation, the results of which are presented in subsequent subsections.

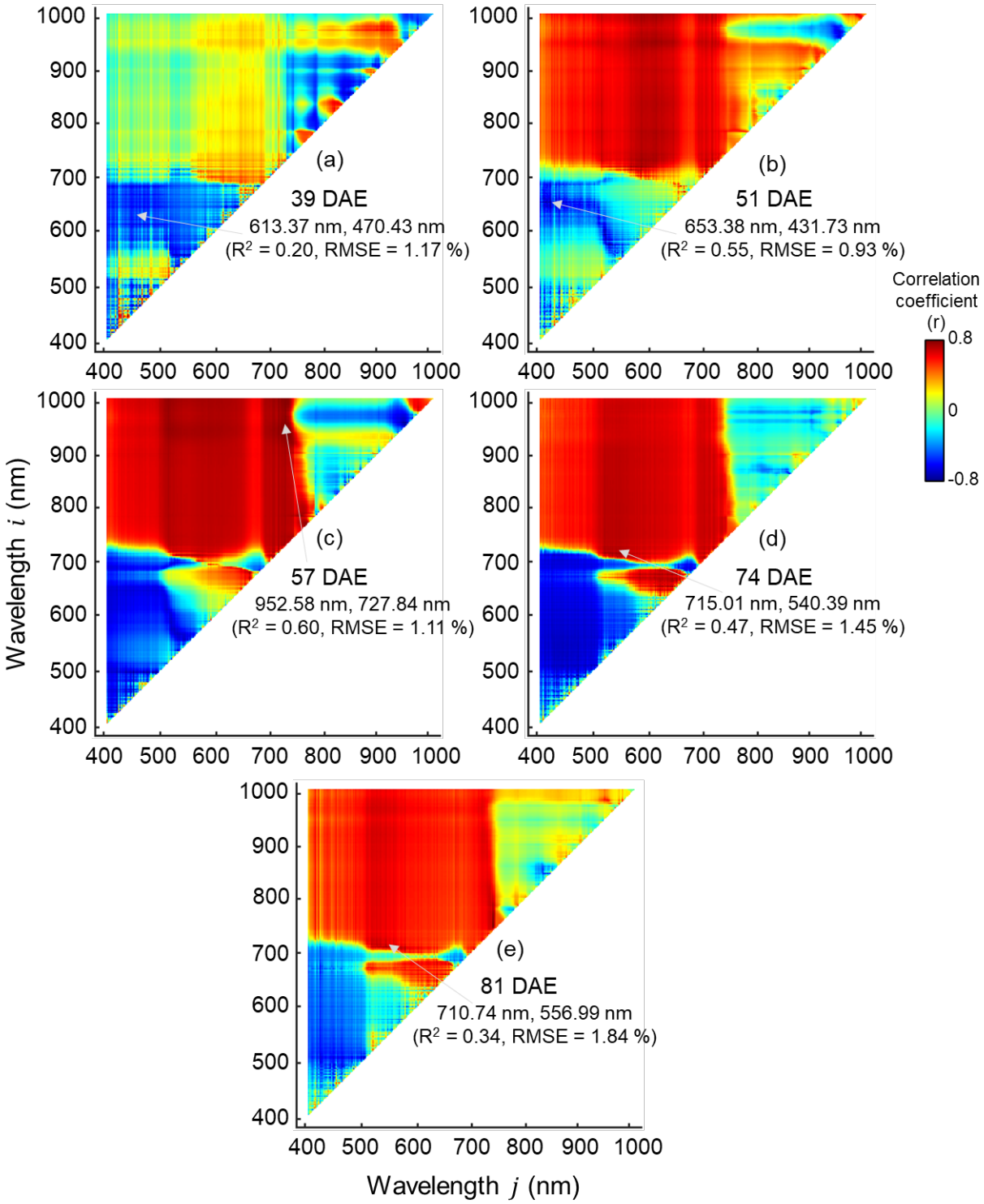

Fig 4. Heatmaps showing the correlation between NDSIs of two-wavelength combinations of hyperspectral datasets with the measured leaf RWC for 39-, 51-, 57-, 74- and 81 DAEs (shown from (a) to (e)). The wavelength combinations with the best linear fit with their R^2 and RMSE values have been indicated for the correlation heatmaps corresponding to each date of data acquisition. NDSI- Normalized differential spectral index.

RF regression

Regression using the RF approach estimated the RWC based on randomly choosing spectral features out of the training hyperspectral dataset (70% of the total dataset) and reducing prediction variance by averaging multiple estimates of these training samples for each epoch. The overall R^2 for model training was observed to be 0.77 with a low RMSE (0.85 %), shown in Fig.

5(a). However, the RWC estimates in cross-validation (R^2 = 0.42, RMSE = 1.25 %, in Fig. 5(b)) were clustered and assumed to be a possible distribution of cross-validated samples into identical learned feature space. Similar results were also obtained with increasing the number of leaf node splits hyperparameter. A high contrast among the training and cross-validation results suggested model overfitting in RF regression owing to high spectral similarities, minuscule noise among a limited number of data samples. This limitation was substantially overcome using GA-PLSR which initially identified the key predictor features subset for modeling RWC estimation.

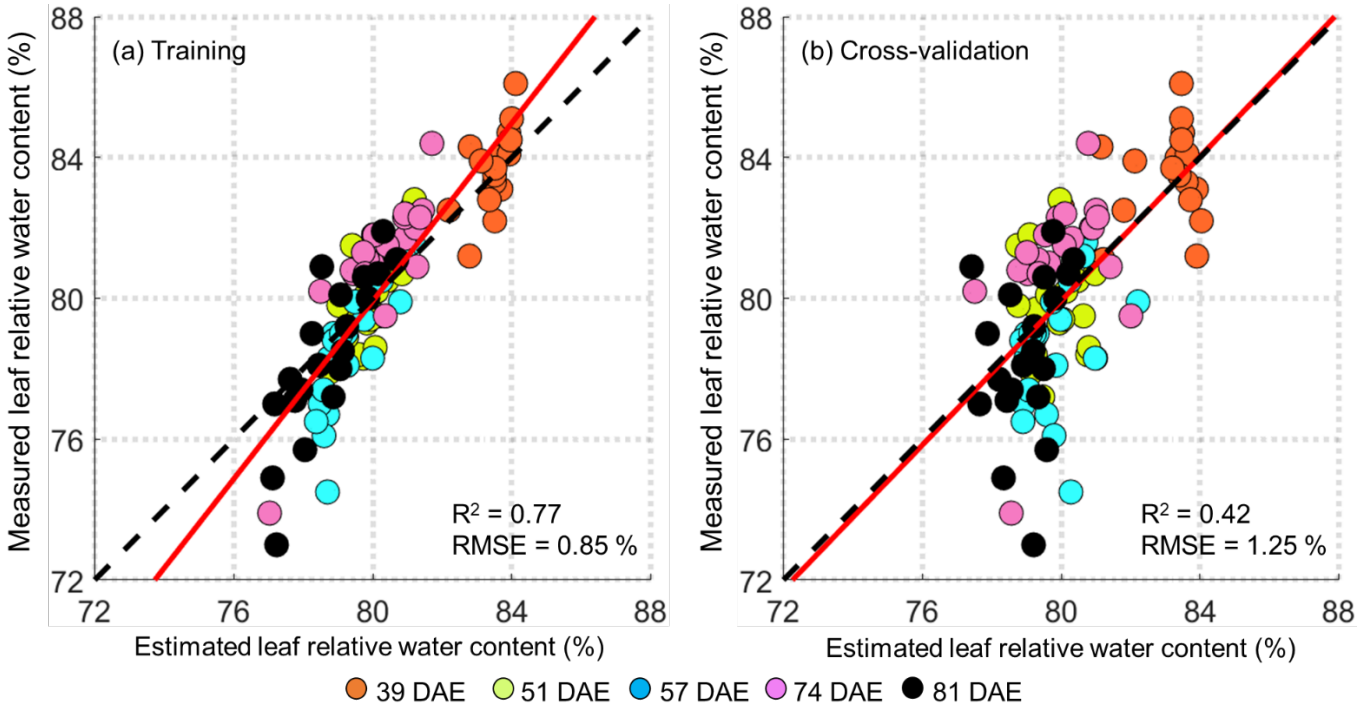

Fig 5. Scatterplots of measured vs. estimated leaf RWC obtained using RF regression for (a) training and (b) cross-validation. The R^2 and RMSE values of the linear fit has been shown displayed for these scatterplots. The markers are colored based on the date of data acquisition. RF- Random forest.

GA-PLSR

GA-PLSR identified key spectral features diagnostic to leaf RWC as a combination of results obtained from spectral and NDSI regression across all spectral acquisition dates. A higher weightage was provided for the 950 – 970 nm spectral region pertaining to hydroxyl (O-H) absorption prevalent in water molecules (Curran, 1989), which had earlier been obtained from NDSI correlation heatmap (Fig. 4(c)).

The identified spectral features used to train the model with 10 PLS components on 70 % of samples indicated a linear fit with R^2 = 0.77 and RMSE = 1.24 % (Fig. 6(a)). The cross-validation results (R^2 = 0.76, RMSE = 1.76 % in Fig. 6(b)) also minimized the contrast with those obtained for model training. Though the RMSE among GA-PLSR model was higher than those obtained from RF regression, there was reduced effect of data clustering. A robust performance was thus observed for GA-PLSR model, that was subsequently used for mapping sesame leaf RWC for UAV-borne hyperspectral images for all acquisition dates. A comparison of performances and mapping leaf water content have been discussed in the next section.

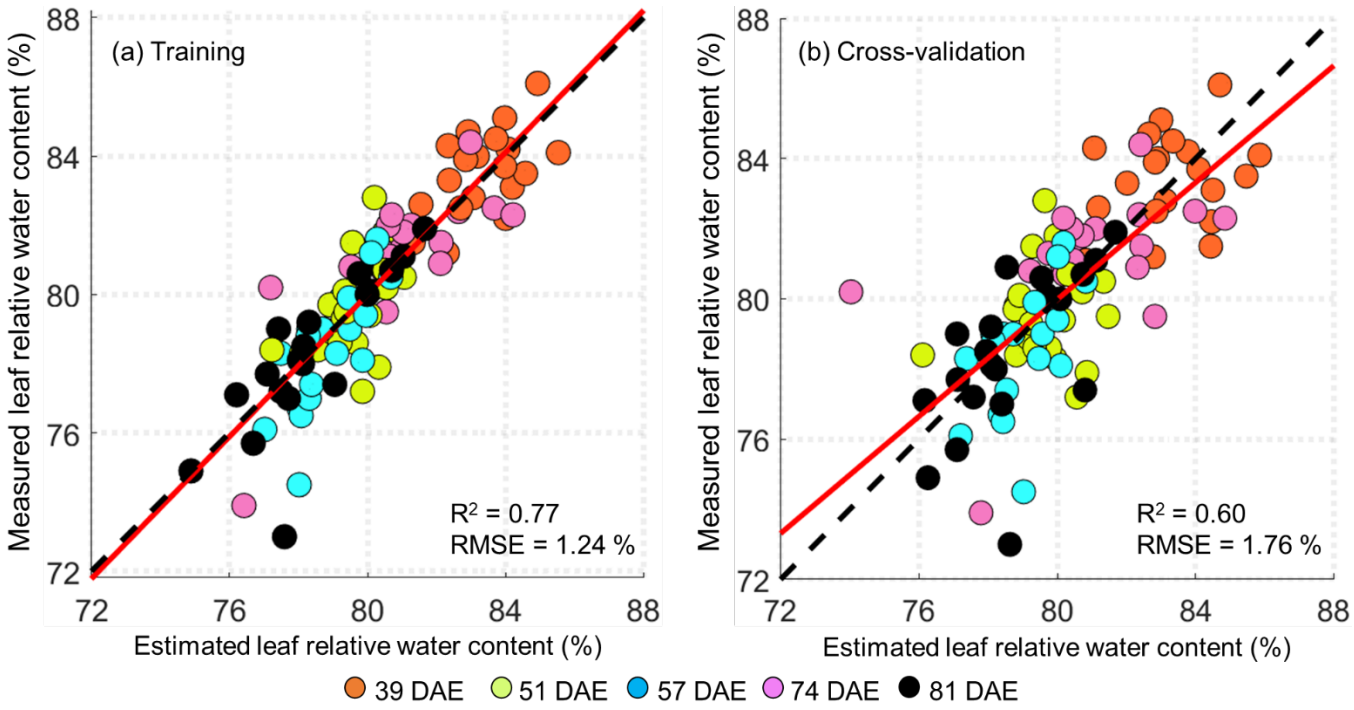

Fig 6. Scatterplots of measured vs. estimated leaf RWC obtained using GA-PLSR for (a) training and (b) cross-validation. The R^2 and RMSE values of the linear fit has been shown displayed for these scatterplots. The markers are colored based on the date of data acquisition. GA-PLSR- Genetic algorithm-inspired partial least squares regression.

DISCUSSION

Performance comparison of models

A comparison of results (Table 1) indicated the estimating ability of discussed models important to spatially map the sesame water status using remotely acquired imagery. Linear regression for each hyperspectral band displayed a max R^2 of 0.30 and min RMSE 1.40 % on only one date (57 DAE). Similarly, linear regression using TIR-derived CWSI had the best fit on 74 DAE (R^2 = 0.25), but the RMSE was minimum for 51 DAE (RMSE = 1.29 %). Regression using NDSI values exhibited a max R^2 = 0.60 on 57 DAE and min RMSE = 0.93 % on 51 DAE, comparable to the GA-PLSR technique. However, these results were obtained only for single date. Comparison among RF (R^2 = 0.42, RMSE = 1.25 %) and GA-PLSR (R^2 = 0.60, RMSE = 1.76 %) revealed the robustness of GA-PLSR for estimating leaf RWC and spatially mapping for sesame plot pixels as discussed in next subsection.

Table 1. Comparison of the performance metrics used in spectral estimation of sesame leaf RWC.

Spectral estimation technique	Max R^2	Observed on	Min RMSE (%)	Observed on
For hyperspectral datasets				
Linear regression	0.30	57 DAE	1.40	57 DAE
NDSI regression	0.60	57 DAE	0.93	51 DAE
RF regression (c.v.)	0.42	All dates	1.25	All dates
GA-PLSR (c.v.)	0.60	All dates	1.76	All dates
For TIR-derived CWSI datasets				
Linear regression	0.25	74 DAE	1.29	51 DAE

Hyperspectral vs. CWSI images for estimating RWC

Assessment of the best performing sesame leaf RWC estimation using TIR-derived CWSI and hyperspectral reflectance images, implemented for 74 DAE of data acquisition, provided a comparable result (Table 2). A plot-wise analysis of mean estimated RWCs and their absolute deviation from measured RWCs indicated higher deviations for sesame plots numbered 2, 13, 15, 16 and 19 estimated from hyperspectral as well as CWSI datasets. A possibility of gradient in irrigation can be assumed for spatial proximity of plots 15, 16 and 19 with reduced RWC estimations. Plots 1, 2, 15, 16 displayed higher deviations for RWCs derived from CWSI image compared to hyperspectral reflectance. This can be attributed to coarser spatial resolution for thermal data acquisition resulting in addition of noise. The standard deviation (s.d.) obtained from the mean estimated values indicated a reliable predictability of leaf RWC from hyperspectral image (s.d. = 1.17) compared to TIR-derived CWSI image (s.d = 1.43). It must be noted that RWC estimation technique implemented using hyperspectral datasets was train-test based on learning spectral features across all data acquisition dates, while using CWSI was based only for 74 DAE.

Table 2. Comparison of measured leaf RWC with mean of RWC estimated using hyperspectral and TIR-derived CWSI imageries acquired on 74 DAE for individual sesame plots. The absolute deviation of mean estimated RWC from measured RWC have been provided for standard deviation (s.d.) analysis.

Plot no.	Measured RWC (in %)	Mean of estimated RWC values per plot (in %)		Absolute deviation of mean estimated RWC from measured RWC (in %)	
		From hyperspectral image	From CWSI image	From hyperspectral image	From CWSI image
1	80.70	81.27	79.76	0.57	0.94
2	84.40	82.77	82.02	1.63	2.38
3	81.00	80.50	80.56	0.5	0.44
4	81.10	80.71	81.37	0.39	0.27
5	82.00	80.82	81.32	1.18	0.68
6	81.70	80.14	81.64	1.56	0.06
7	79.50	80.34	78.89	0.84	0.61
8	81.50	82.57	82.18	1.07	0.68
9	80.20	79.27	79.34	0.93	0.86
10	81.80	81.10	81.81	0.7	0.01
11	82.00	80.63	81.78	1.37	0.22
12	80.80	79.18	80.65	1.62	0.15
13	81.30	79.38	79.81	1.92	1.49
14	82.50	84.34	82.31	1.84	0.19
15	73.90	79.02	80.25	5.12	6.35
16	80.90	82.07	82.14	1.17	1.24
17	82.30	80.80	81.23	1.5	1.07
18	80.70	79.30	82.08	1.4	1.38
19	82.40	78.11	79.76	4.29	2.64
20	82.30	83.40	81.76	1.1	0.54
			s.d. for all sesame plots	1.17	1.43

Summary and Conclusion

In this study, leaf RWC was estimated from hyperspectral and thermal UAV-borne imagery of an experimental sesame field using paradigms of spectral estimation techniques- regression using spectral bands, NDSIs, random forest and GA-PLSR. Hyperspectral band based linear regression identified one wavelength having a correlation with RWC. TIR band provided a comparatively reduced model fit than hyperspectral bands in the VIS and NIR regions. Regression using NDSIs highlighted two-band combinations that provided a best fit for estimating water content. These techniques, however, provided the best results only for one date of data acquisition. ML models- RF regression and GA-PLSR iteratively trained on 70 % and cross-validated on 30 % of dataset performed better than the previous-mentioned techniques. RF regression had reduced performance metrics due to a limited number of data samples used. However, the GA-PLSR showed a stable result with minimized contrast between training and cross-validation.

The results obtained were analyzed and the best approaches were examined for UAV-borne imagery on one of the data acquisition dates (74 DAE) to map the average leaf RWC for each sesame plot. It was observed that both hyperspectral dataset-based GA-PLSR and thermal dataset-based linear estimation performed comparatively well, though the variation among the RWC estimation (represented through s.d.) was lesser for hyperspectral estimations. It must be further noted that the thermal datasets provided best results only at one date. This expresses the robustness of GA-PLSR and ML models for remote estimation of crop water status.

Further studies would be conducted on the ability of remote estimation techniques to distinguish the irrigated and stressed crops for a growing season. This could provide more insights on the crop-water dynamics and give informed decisions to growers and producers for an irrigation management with reduced agricultural carbon footprint.

Acknowledgments

The authors would like to thank Prof. Zvi Peleg, Idan Sabag and Yaron Gadri from the Robert H. Smith Faculty of Agriculture, Food and Environment, The Hebrew University of Jerusalem, Rehovot, Israel for using their Sesame seeds and supporting agronomical decisions.

References

Alchanatis, V., Cohen, Y., Cohen, S., Moller, M., Sprinstin, M., Meron, M., et al. (2010). Evaluation of different approaches for estimating and mapping crop water status in cotton with thermal imaging. *Precision Agriculture*, *11*(1), 27–41. https://doi.org/10.1007/s11119-009-9111-7

Ceccato, P., Flasse, S., Tarantola, S., Jacquemoud, S., & Grégoire, J.-M. (2001). Detecting vegetation leaf water content using reflectance in the optical domain. *Remote Sensing of Environment*, *77*(1), 22–33. https://doi.org/10.1016/S0034-4257(01)00191-2

Clevers, J. G. P. W., Kooistra, L., & Schaepman, M. E. (2010). Estimating canopy water content using hyperspectral remote sensing data. *International Journal of Applied Earth Observation and Geoinformation*, *12*(2), 119–125. https://doi.org/10.1016/j.jag.2010.01.007

Curran, P. J. (1989). Remote Sensing of Foliar Chemistry. *Remote Sensing of Environment*, *30*(3), 271–278. https://doi.org/10.1016/0034-4257(89)90069-2

Fabre, S., Lesaignoux, A., Olioso, A., & Briottet, X. (2011). Influence of water content on spectral reflectance of leaves in the 3-15-µm domain. *IEEE Geoscience and Remote Sensing Letters*, *8*(1), 143–147. https://doi.org/10.1109/LGRS.2010.2053518

Gao, Y., Walker, J. P., Allahmoradi, M., Monerris, A., Ryu, D., & Jackson, T. J. (2015). Optical sensing of vegetation water content: A synthesis study. *IEEE Journal of Selected Topics in Applied Earth Observations and Remote Sensing*, *8*(4), 1456–1464. https://doi.org/10.1109/JSTARS.2015.2398034

Herrmann, I., Vosberg, S. K., Ravindran, P., Singh, A., Chang, H. X., Chilvers, M. I., et al. (2018).

Leaf and canopy level detection of Fusarium virguliforme (sudden death syndrome) in soybean. *Remote Sensing*, *10*(3), 426. https://doi.org/10.3390/rs10030426

Hsiao, T. C., & Acevedo, E. (1974). Plant responses to water deficits, water-use efficiency, and drought resistance. *Agricultural Meteorology*, *14*(1–2), 59–84. https://doi.org/10.1016/0002-1571(74)90011-9

Huang, Y., Walker, J. P., Gao, Y., Wu, X., & Monerris, A. (2016). Estimation of vegetation water content from the radar vegetation index at L-Band. *IEEE Transactions on Geoscience and Remote Sensing*, *54*(2), 981–989. https://doi.org/10.1109/TGRS.2015.2471803

Hunt, E. R., Li, L., Yilmaz, M. T., & Jackson, T. J. (2011). Comparison of vegetation water contents derived from shortwave-infrared and passive-microwave sensors over central Iowa. *Remote Sensing of Environment*, *115*(9), 2376–2383. https://doi.org/10.1016/j.rse.2011.04.037

Jackson, R. D. (1982). Canopy temperature and crop water stress. In D. I. Hillel (Ed.), Advances in irrigation (Vol. 1, pp. 43–85). New York: Academic Press.

Langford, E. (2006). Quartiles in elementary statistics. *Journal of Statistics Education*, *14*(3). https://doi.org/10.1080/10691898.2006.11910589

Leardi, R., Boggia, R., & Terrile, M. (1992). Genetic algorithms as a strategy for feature selection. *Journal of Chemometrics*, *6*(5), 267–281. https://doi.org/10.1002/cem.1180060506

Leardi, Riccardo, & Lupiáñez González, A. (1998). Genetic algorithms applied to feature selection in PLS regression: How and when to use them. *Chemometrics and Intelligent Laboratory Systems*, *41*(2), 195–207. https://doi.org/10.1016/S0169-7439(98)00051-3

Merlin, O., Al Bitar, A., Walker, J. P., & Kerr, Y. (2010). An improved algorithm for disaggregating microwave-derived soil moisture based on red, near-infrared and thermal-infrared data. *Remote Sensing of Environment*, *114*(10), 2305–2316. https://doi.org/10.1016/j.rse.2010.05.007

Neinavaz, E., Skidmore, A. K., Darvishzadeh, R., & Groen, T. A. (2017). Retrieving vegetation canopy water content from hyperspectral thermal measurements. *Agricultural and Forest Meteorology*, *247*, 365–375. https://doi.org/10.1016/j.agrformet.2017.08.020

Pehuelas, J., Gamon, J. A., Griffin, K. L., & Field II, C. B. (1993). Assessing Community Type, Plant Biomass, Pigment Composition, and Photosynthetic Efficiency of Aquatic Vegetation from Spectral Reflectance*. *Remote Sensing of Environment*, *46*(2), 110–118. https://doi.org/10.1016/0034-4257(93)90088-F

Penuelas, J., Pinol, J., Ogaya, R., & Filella, I. (1997). Estimation of plant water concentration by the reflectance Water Index WI (R900/R970). *International Journal of Remote Sensing*, *18*(13), 2869–2875. https://doi.org/10.1080/014311697217396

Raj, R., Walker, J. P., Vinod, V., Pingale, R., Naik, B., & Jagarlapudi, A. (2021). Leaf water content estimation using top-of-canopy airborne hyperspectral data. *International Journal of Applied Earth Observation and Geoinformation*, *102*, 102393. https://doi.org/10.1016/j.jag.2021.102393

Raya-Sereno, M. D., Camino, C., Pancorbo, J. L., Alonso-Ayuso, M., Gabriel, J. L., Beck, P. S. A., & Quemada, M. (2024). Assessing wheat genotype response under combined nitrogen and water stress scenarios coupling high-resolution optical and thermal sensors with radiative transfer models. *European Journal of Agronomy*, *154*, 127102. https://doi.org/10.1016/j.eja.2024.127102

Sahoo, M. M., Perach, O., Shachter, A., Gonda, I., Porwal, A., Dudai, N., & Herrmann, I. (2022). Spectral estimation of carnosic acid content in in vivo rosemary plants. *Industrial Crops and Products*, *187*(A), 115292. https://doi.org/10.1016/j.indcrop.2022.115292

Savitzky, A., & Golay, M. J. E. (1964). Smoothing and Differentiation of Data by Simplified Least Squares Procedures. *Analytical Chemistry*, *36*(8), 1627–1639. https://doi.org/10.1021/ac60214a047

Srikanth, P., Chakraborty, A., Murthy, C.S. (2021). Crop Monitoring Using Microwave Remote

Sensing. In: Mitran, T., Meena, R.S., Chakraborty, A. (eds) Geospatial Technologies for Crops and Soils. Springer, Singapore. https://doi.org/10.1007/978-981-15-6864-0_5

Thenkabail, P. S., Smith, R. B., & De Pauw, E. (2000). Hyperspectral vegetation indices and their relationships with agricultural crop characteristics. *Remote Sensing of Environment*, *71*(2), 158–182. https://doi.org/10.1016/S0034-4257(99)00067-X

Ullah, S., Skidmore, A. K., Naeem, M., & Schlerf, M. (2012). An accurate retrieval of leaf water content from mid to thermal infrared spectra using continuous wavelet analysis. *Science of the Total Environment*, *437*, 145–152. https://doi.org/10.1016/j.scitotenv.2012.08.025

Yilmaz, M. T., Hunt, E. R., & Jackson, T. J. (2008). Remote sensing of vegetation water content from equivalent water thickness using satellite imagery. *Remote Sensing of Environment*, *112*(5), 2514–2522. https://doi.org/10.1016/j.rse.2007.11.014